The Astrophysical Journal, 892:53 (11pp), 2020 March 20 https://doi.org/10.3847/1538-4357/ab791d

A Search for IceCube Events in the Direction of ANITA Neutrino Candidates

M. G. Aartsen[1], M. Ackermann[2], J. Adams[1], J. A. Aguilar[3], M. Ahlers[4], M. Ahrens[5], C. Alispach[6], K. Andeen[7], T. Anderson[8], I. Ansseau[3], G. Anton[9], C. Argüelles[10], J. Auffenberg[11], S. Axani[10], P. Backes[11], H. Bagherpour[1], X. Bai[12], A. Balagopal V.[13], A. Barbano[6], S. W. Barwick[14], B. Bastian[2], V. Baum[15], S. Baur[3], R. Bay[16], J. J. Beatty[17,18], K.-H. Becker[19], J. Becker Tjus[20], S. BenZvi[21], D. Berley[22], E. Bernardini[2], D. Z. Besson[23], G. Binder[16,24], D. Bindig[19], E. Blaufuss[22], S. Blot[2], C. Bohm[5], S. Böser[15], O. Botner[25], J. Böttcher[11], E. Bourbeau[4], J. Bourbeau[26], F. Bradascio[2], J. Braun[26], S. Bron[6], J. Brostean-Kaiser[2], A. Burgman[25], J. Buscher[11], R. S. Busse[27], T. Carver[6], C. Chen[28], E. Cheung[22], D. Chirkin[26], S. Choi[29], K. Clark[30], L. Classen[27], A. Coleman[31], G. H. Collin[10], J. M. Conrad[10], P. Coppin[32], P. Correa[32], D. F. Cowen[8,33], R. Cross[21], P. Dave[28], C. De Clercq[32], J. J. DeLaunay[8], H. Dembinski[31], K. Deoskar[5], S. De Ridder[34], P. Desiati[26], K. D. de Vries[32], G. de Wasseige[32], M. de With[35], T. DeYoung[36], A. Diaz[10], J. C. Díaz-Vélez[26], H. Dujmovic[13], M. Dunkman[8], E. Dvorak[12], B. Eberhardt[26], T. Ehrhardt[15], P. Eller[8], R. Engel[13], P. A. Evenson[31], S. Fahey[26], A. R. Fazely[37], J. Felde[22], K. Filimonov[16], C. Finley[5], D. Fox[33], A. Franckowiak[2], E. Friedman[22], A. Fritz[15], T. K. Gaisser[31], J. Gallagher[38], E. Ganster[11], S. Garrappa[2], L. Gerhardt[24], K. Ghorbani[26], T. Glauch[39], T. Glüsenkamp[9], A. Goldschmidt[24], J. G. Gonzalez[31], D. Grant[36], Z. Griffith[26], S. Griswold[21], M. Günder[11], M. Gündüz[20], C. Haack[11], A. Hallgren[25], R. Halliday[36], L. Halve[11], F. Halzen[26], K. Hanson[26], A. Haungs[13], D. Hebecker[35], D. Heereman[3], P. Heix[11], K. Helbing[19], R. Hellauer[22], F. Henningsen[39], S. Hickford[19], J. Hignight[40], G. C. Hill[41], K. D. Hoffman[22], R. Hoffmann[19], T. Hoinka[42], B. Hokanson-Fasig[26], K. Hoshina[26], F. Huang[8], M. Huber[39], T. Huber[2,13], K. Hultqvist[5], M. Hünnefeld[42], R. Hussain[26], S. In[29], N. Iovine[3], A. Ishihara[43], G. S. Japaridze[44], M. Jeong[29], K. Jero[26], B. J. P. Jones[45], F. Jonske[11], R. Joppe[11], D. Kang[13], W. Kang[29], A. Kappes[27], D. Kappesser[15], T. Karg[2], M. Karl[39], A. Karle[26], U. Katz[9], M. Kauer[26], J. L. Kelley[26], A. Kheirandish[26], J. Kim[29], T. Kintscher[2], J. Kiryluk[46], T. Kittler[9], S. R. Klein[16,24], R. Koirala[31], H. Kolanoski[35], L. Köpke[15], C. Kopper[36], S. Kopper[47], D. J. Koskinen[4], M. Kowalski[2,35], K. Krings[39], G. Krückl[15], N. Kulacz[40], N. Kurahashi[48], A. Kyriacou[41], J. L. Lanfranchi[8], M. J. Larson[22], F. Lauber[19], J. P. Lazar[26], K. Leonard[26], A. Leszczyńska[13], M. Leuermann[11], Q. R. Liu[26], E. Lohfink[15], C. J. Lozano Mariscal[27], L. Lu[43], F. Lucarelli[6], J. Lünemann[32], W. Luszczak[26], Y. Lyu[16,24], W. Y. Ma[2], J. Madsen[49], G. Maggi[32], K. B. M. Mahn[36], Y. Makino[43], P. Mallik[11], K. Mallot[26], S. Mancina[26], I. C. Mariş[3], R. Maruyama[50], K. Mase[43], R. Maunu[22], F. McNally[51], K. Meagher[26], M. Medici[4], A. Medina[18], M. Meier[42], S. Meighen-Berger[39], G. Merino[26], T. Meures[3], J. Micallef[36], D. Mockler[3], G. Momenté[15], T. Montaruli[6], R. W. Moore[40], R. Morse[26], M. Moulai[10], P. Muth[11], R. Nagai[43], U. Naumann[19], G. Neer[36], H. Niederhausen[39], M. U. Nisa[36], S. C. Nowicki[36], D. R. Nygren[24], A. Obertacke Pollmann[19], M. Oehler[13], A. Olivas[22], A. O'Murchadha[3], E. O'Sullivan[5], T. Palczewski[16,24], H. Pandya[31], D. V. Pankova[8], N. Park[26], P. Peiffer[15], C. Pérez de los Heros[25], S. Philippen[11], D. Pieloth[42], E. Pinat[3], A. Pizzuto[26], M. Plum[7], A. Porcelli[34], P. B. Price[16], G. T. Przybylski[24], C. Raab[3], A. Raissi[1], M. Rameez[4], L. Rauch[2], K. Rawlins[52], I. C. Rea[39], R. Reimann[11], B. Relethford[48], M. Renschler[13], G. Renzi[3], E. Resconi[39], W. Rhode[42], M. Richman[48], S. Robertson[24], M. Rongen[11], C. Rott[29], T. Ruhe[42], D. Ryckbosch[34], D. Rysewyk[36], I. Safa[26], S. E. Sanchez Herrera[36], A. Sandrock[42], J. Sandroos[15], M. Santander[47], S. Sarkar[53], S. Sarkar[40], K. Satalecka[2], M. Schaufel[11], H. Schieler[13], P. Schlunder[42], T. Schmidt[22], A. Schneider[26], J. Schneider[9], F. G. Schröder[13,31], L. Schumacher[11], S. Sclafani[48], S. Seunarine[49], S. Shefali[11], M. Silva[26], R. Snihur[26], J. Soedingrekso[42], D. Soldin[31], M. Song[22], G. M. Spiczak[49], C. Spiering[2], J. Stachurska[2], M. Stamatikos[18], T. Stanev[31], R. Stein[2], J. Stettner[11], A. Steuer[15], T. Stezelberger[24], R. G. Stokstad[24], A. Stößl[43], N. L. Strotjohann[2], T. Stürwald[11], T. Stuttard[4], G. W. Sullivan[22], I. Taboada[28], F. Tenholt[20], S. Ter-Antonyan[37], A. Terliuk[2], S. Tilav[31], K. Tollefson[36], L. Tomankova[20], C. Tönnis[54], S. Toscano[3], D. Tosi[26], A. Trettin[2], M. Tselengidou[9], C. F. Tung[28], A. Turcati[39], R. Turcotte[13], C. F. Turley[8], B. Ty[26], E. Unger[25], M. A. Unland Elorrieta[27], M. Usner[2], J. Vandenbroucke[26], W. Van Driessche[34], D. van Eijk[26], N. van Eijndhoven[32], J. van Santen[2], S. Verpoest[34], M. Vraeghe[34], C. Walck[5], A. Wallace[41], M. Wallraff[11], N. Wandkowsky[26], T. B. Watson[45], C. Weaver[40], A. Weindl[13], M. J. Weiss[8], J. Weldert[15], C. Wendt[26], J. Werthebach[26], B. J. Whelan[41], N. Whitehorn[55], K. Wiebe[15], C. H. Wiebusch[11], L. Wille[26], D. R. Williams[47], L. Wills[48], M. Wolf[39], J. Wood[26], T. R. Wood[40], K. Woschnagg[16], G. Wrede[9], D. L. Xu[26], X. W. Xu[37], Y. Xu[46], J. P. Yanez[40], G. Yodh[14], S. Yoshida[43], T. Yuan[26], and M. Zöcklein[11]

Icecube Collaboration

[1] Department of Physics and Astronomy, University of Canterbury, Private Bag 4800, Christchurch, New Zealand
[2] DESY, D-15738 Zeuthen, Germany
[3] Université Libre de Bruxelles, Science Faculty CP230, B-1050 Brussels, Belgium
[4] Niels Bohr Institute, University of Copenhagen, DK-2100 Copenhagen, Denmark
[5] Oskar Klein Centre and Department of Physics, Stockholm University, SE-10691 Stockholm, Sweden
[6] Département de physique nucléaire et corpusculaire, Université de Genève, CH-1211 Genève, Switzerland
[7] Department of Physics, Marquette University, Milwaukee, WI 53201, USA
[8] Department of Physics, Pennsylvania State University, University Park, PA 16802, USA
[9] Erlangen Centre for Astroparticle Physics, Friedrich-Alexander-Universität Erlangen-Nürnberg, D-91058 Erlangen, Germany
[10] Department of Physics, Massachusetts Institute of Technology, Cambridge, MA 02139, USA
[11] III. Physikalisches Institut, RWTH Aachen University, D-52056 Aachen, Germany
[12] Physics Department, South Dakota School of Mines and Technology, Rapid City, SD 57701, USA
[13] Karlsruhe Institute of Technology, Institut für Kernphysik, D-76021 Karlsruhe, Germany
[14] Department of Physics and Astronomy, University of California, Irvine, CA 92697, USA

[15] Institute of Physics, University of Mainz, Staudinger Weg 7, D-55099 Mainz, Germany
[16] Department of Physics, University of California, Berkeley, CA 94720, USA
[17] Department of Astronomy, Ohio State University, Columbus, OH 43210, USA
[18] Department of Physics and Center for Cosmology and Astro-Particle Physics, Ohio State University, Columbus, OH 43210, USA
[19] Department of Physics, University of Wuppertal, D-42119 Wuppertal, Germany
[20] Fakultät für Physik & Astronomie, Ruhr-Universität Bochum, D-44780 Bochum, Germany
[21] Department of Physics and Astronomy, University of Rochester, Rochester, NY 14627, USA
[22] Department of Physics, University of Maryland, College Park, MD 20742, USA
[23] Department of Physics and Astronomy, University of Kansas, Lawrence, KS 66045, USA[57]
[24] Lawrence Berkeley National Laboratory, Berkeley, CA 94720, USA
[25] Department of Physics and Astronomy, Uppsala University, Box 516, SE-75120 Uppsala, Sweden
[26] Department of Physics and Wisconsin IceCube Particle Astrophysics Center, University of Wisconsin, Madison, WI 53706, USA[58]
[27] Institut für Kernphysik, Westfälische Wilhelms-Universität Münster, D-48149 Münster, Germany
[28] School of Physics and Center for Relativistic Astrophysics, Georgia Institute of Technology, Atlanta, GA 30332, USA
[29] Department of Physics, Sungkyunkwan University, Suwon 16419, Republic of Korea
[30] SNOLAB, 1039 Regional Road 24, Creighton Mine 9, Lively, ON, P3Y 1N2, Canada
[31] Bartol Research Institute and Department of Physics and Astronomy, University of Delaware, Newark, DE 19716, USA
[32] Vrije Universiteit Brussel (VUB), Dienst ELEM, B-1050 Brussels, Belgium
[33] Department of Astronomy and Astrophysics, Pennsylvania State University, University Park, PA 16802, USA
[34] Department of Physics and Astronomy, University of Gent, B-9000 Gent, Belgium
[35] Institut für Physik, Humboldt-Universität zu Berlin, D-12489 Berlin, Germany
[36] Department of Physics and Astronomy, Michigan State University, East Lansing, MI 48824, USA
[37] Department of Physics, Southern University, Baton Rouge, LA 70813, USA
[38] Department of Astronomy, University of Wisconsin, Madison, WI 53706, USA
[39] Physik-department, Technische Universität München, D-85748 Garching, Germany
[40] Department of Physics, University of Alberta, Edmonton, AB, T6G 2E1, Canada
[41] Department of Physics, University of Adelaide, Adelaide, 5005, Australia
[42] Department of Physics, TU Dortmund University, D-44221 Dortmund, Germany
[43] Department of Physics and Institute for Global Prominent Research, Chiba University, Chiba 263-8522, Japan
[44] CTSPS, Clark-Atlanta University, Atlanta, GA 30314, USA
[45] Department of Physics, University of Texas at Arlington, 502 Yates Street, Science Hall Room 108, Box 19059, Arlington, TX 76019, USA
[46] Department of Physics and Astronomy, Stony Brook University, Stony Brook, NY 11794-3800, USA
[47] Department of Physics and Astronomy, University of Alabama, Tuscaloosa, AL 35487, USA
[48] Department of Physics, Drexel University, 3141 Chestnut Street, Philadelphia, PA 19104, USA
[49] Department of Physics, University of Wisconsin, River Falls, WI 54022, USA
[50] Department of Physics, Yale University, New Haven, CT 06520, USA
[51] Department of Physics, Mercer University, Macon, GA 31207-0001, USA
[52] Department of Physics and Astronomy, University of Alaska Anchorage, 3211 Providence Drive, Anchorage, AK 99508, USA
[53] Department of Physics, University of Oxford, Parks Road, Oxford OX1 3PU, UK
[54] Institute of Basic Science, Sungkyunkwan University, Suwon 16419, Republic of Korea
[55] Department of Physics and Astronomy, UCLA, Los Angeles, CA 90095, USA; analysis@icecube.wisc.edu
Received 2020 January 6; revised 2020 February 19; accepted 2020 February 20; published 2020 March 27

Abstract

During the first three flights of the Antarctic Impulsive Transient Antenna (ANITA) experiment, the collaboration detected several neutrino candidates. Two of these candidate events were consistent with an ultra-high-energy upgoing air shower and compatible with a tau neutrino interpretation. A third neutrino candidate event was detected in a search for Askaryan radiation in the Antarctic ice, although it is also consistent with the background expectation. The inferred emergence angle of the first two events is in tension with IceCube and ANITA limits on isotropic cosmogenic neutrino fluxes. Here we test the hypothesis that these events are astrophysical in origin, possibly caused by a point source in the reconstructed direction. Given that any ultra-high-energy tau neutrino flux traversing the Earth should be accompanied by a secondary flux in the TeV–PeV range, we search for these secondary counterparts in 7 yr of IceCube data using three complementary approaches. In the absence of any significant detection, we set upper limits on the neutrino flux from potential point sources. We compare these limits to ANITA's sensitivity in the same direction and show that an astrophysical explanation of these anomalous events under standard model assumptions is severely constrained regardless of source spectrum.

Unified Astronomy Thesaurus concepts: Neutrino astronomy (1100); High energy astrophysics (739)

1. Introduction

Ever since the detection of high-energy neutrinos of cosmic origin by IceCube in 2013 (Aartsen et al. 2013a), experiments and theoreticians alike have continued to probe the nonthermal processes in the universe to understand their origins. The bulk of these astrophysical neutrinos are believed to be created in hadronic interactions between cosmic rays and ambient matter or radiation fields in the vicinity of cosmic accelerators (Gaisser et al. 1995), and their detections can be used to point back to the acceleration sites. Although the first evidence of a neutrino point source, the blazar TXS 0506+056, was reported in 2018 (Aartsen et al. 2018c, 2018d), the overwhelming majority of the measured neutrino flux remains unexplained.

[56] Also at Università di Padova, I-35131 Padova, Italy.
[57] Also at National Research Nuclear University, Moscow Engineering Physics Institute (MEPhI), Moscow 115409, Russia.
[58] Earthquake Research Institute, University of Tokyo, Bunkyo, Tokyo 113-0032, Japan.

Table 1
Properties of the Neutrino Candidate Events from the First Three Flights of ANITA from Gorham et al. (2018a, 2016, 2018b)

	AAE-061228	AAE-141220	AAC-150108
Event, flight	3985267, ANITA-I	15717147, ANITA-III	83139414, ANITA-III
Detection channel	Geomagnetic	Geomagnetic	Askaryan
Date, time (UTC)	2006-12-28, 00:33:20	2014-12-20, 08:33:22.5	2015-01-08, 19:04:24.237
R.A., decl. (J2000)[a]	$282.^{\circ}14$, $+20.^{\circ}33$	$50.^{\circ}78$, $+38.^{\circ}65$	$171.^{\circ}45$, $+16.^{\circ}30$
Localization uncertainty[b]	$1.^{\circ}5 \times 1.^{\circ}5$, $0.^{\circ}0$	$1.^{\circ}5 \times 1.^{\circ}5$, $0.^{\circ}0$	$5.^{\circ}0 \times 1.^{\circ}0$, $+73.^{\circ}7$
Reconstructed energy (EeV)	0.6 ± 0.4	$0.56^{+0.30}_{-0.20}$	$\geqslant 10$
Earth chord length (km)	5740 ± 60	7210 ± 55	⋯

Notes. The two AAEs are consistent with a steeply upgoing ν_τ interpretation.
[a] Sky coordinates are projections from event arrival angles at ANITA.
[b] Expressed as major- and minor-axis standard deviations, followed by the position angle. This angle describes the rotation of the major axis relative to the north celestial pole turning positive into R.A.

Additionally, another population of neutrinos could exist at extremely high energies. Cosmogenic neutrinos are believed to be the result of interactions between ultra-high-energy (UHE) cosmic rays (CRs) and the cosmic microwave background (CMB; Greisen 1966; Zatsepin & Kuzmin 1966). This population is expected to manifest as an isotropic flux at Earth, as cosmic-ray primaries can travel outside of the vicinity of their accelerators before interacting with the CMB.

The Antarctic Impulsive Transient Antenna (ANITA) experiment is a balloon experiment designed with the primary purpose of detecting the UHE cosmogenic neutrino flux (Gorham et al. 2009; Hoover et al. 2010; Gorham et al. 2018a). Although this is the experiment's primary scientific goal, it is sensitive to a wide array of impulsive radio signals, and the experiment's first three flights have resulted in a few interesting detections. In this work, we focus on three events observed by ANITA in its searches, all of which have potential neutrino interpretations. Throughout this work, we refer to and explore them as "neutrino candidates." In the third flight, one Askaryan neutrino candidate (AAC) event was simultaneously identified in one analysis searching for Askaryan emission (Askar'yan 1962) and found to be subthreshold in another. This Earth-skimming event has a signal shape consistent with impulsive broadband emission characteristic of a neutrino origin, and it also came from a location on the continent consistent with simulated distribution of neutrinos of all flavors (Gorham et al. 2018a). However, the detection of one candidate event is consistent with the background-level estimates of $0.7^{+0.5}_{-0.3}$ for these analyses. ANITA also reported two additional events, each consistent with an astrophysical ν_τ emerging from the Earth (Gorham et al. 2016, 2018b). In this scenario, a ν_τ undergoes a charged-current interaction with a nucleus in the Earth. The τ-lepton produced in this interaction subsequently decays in the atmosphere, producing an extensive air shower (EAS). The polarity of the radio signal makes it possible to identify and reject downward-moving cosmic-ray-induced EASs, as the radio signals of these EASs acquire a phase reversal (opposite polarity) from reflection off the Antarctic ice, while an upgoing τ-induced EAS does not acquire this phase reversal. For a complete list of details of these events, see Table 1.

The interpretation of these events as extremely high-energy upgoing neutrinos poses many challenges under standard model assumptions. First, from the observation angles and reconstructed energies of the anomalous ANITA events (AAEs), neutrinos are extremely unlikely to traverse the long chord lengths (Gorham et al. 2016), even after accounting for the probability increase due to ν_τ regeneration. Second, if these events are of cosmogenic origin, they would imply fluxes that are in severe tension with limits set by multiple experiments (Aab et al. 2015; Aartsen et al. 2016a, 2018b; Zas 2018), as well as a self-inconsistency from ANITA data alone. For an isotropic flux of cosmogenic neutrinos, ANITA should have detected many more events at other elevation angles than those of the AAEs, as the detector differential acceptance changes with the observation angle (Romero-Wolf et al. 2019).

On the other hand, if the origin of the AAE is considered to be from individual cosmic accelerators, there is no inconsistency with diffuse extremely high-energy flux limits. This is especially true for accelerators with short characteristic timescales of emission, as many current limits on neutrino point sources are for integrated emission over various experiments' lifetimes (Aartsen et al. 2019); in addition, the acceptance of ANITA to a specific location on the sky changes throughout the detector's flight. If we assume that ANITA detected single events of 1 EeV from a cosmic accelerator with an $E^{-\gamma}$ emission power-law spectrum, then we should also expect a larger flux of neutrinos at TeV–PeV energies, where IceCube will be sensitive. A significant correlation between IceCube and ANITA data would not only provide evidence for a neutrino point source, it would also eliminate nonastrophysical explanations of AAEs, such as background and systematics or nonastrophysical models that invoke physics beyond the standard model.

The focus of this work is to use IceCube to investigate the hypothesis that the ANITA events were from neutrino point sources, considering several neutrino emission time profiles. In Section 2 we discuss the IceCube Neutrino Observatory and the event samples used for these analyses. In Section 3 we describe the analysis techniques and summarize the results in Section 4. In Sections 5 and 6 we investigate neutrino propagation through large Earth chord lengths to discuss the implications of our results.

2. Data Sample

IceCube is a cubic-kilometer neutrino detector with 5160 digital optical modules (DOMs) instrumented on 86 cable strings in the clear glacial ice at the geographic South Pole between depths of 1450 and 2450 m (Achterberg et al. 2006; Aartsen et al. 2017b). Neutrinos are detected through the Cerenkov radiation emitted by secondary particles produced by neutrino interactions in the surrounding ice or bedrock. Each DOM consists of a 10 inch photomultiplier tube, onboard

readout electronics, and a high-voltage board, all contained in a pressurized spherical glass container (Abbasi et al. 2009, 2010). Parameterization of the scattering and absorption of the glacial ice allows for accurate energy and directional reconstruction of neutrino events (Aartsen et al. 2013b).

The improved reconstruction techniques adopted to create the event selection (Carver 2019; Aartsen et al. 2020) include updates in the direction reconstruction (Ahrens et al. 2004; Aartsen et al. 2014a) to use information on the deposited event energy in the detector. The median angular resolution benefits from a 10% improvement above 10 TeV (where it is smaller than $0.^{\circ}60$) compared to previous selections (Aartsen et al. 2017a).

While in the southern sky, the trigger rate is dominated by atmospheric muons from cosmic-ray air showers, all of the ANITA candidates have best-fit directions in the northern sky. Here the Earth attenuates the majority of the atmospheric muon signal, and the background at the final selection level in the northern sky is dominated by atmospheric muon neutrinos from cosmic-ray air showers (Haack & Wiebusch 2018). Poorly reconstructed atmospheric muons from the southern sky, as well as neutrino-induced cascades, are also nonnegligible backgrounds in this region of the sky and are removed using a multivariate boosted decision tree trained to distinguish between neutrino-induced muon tracks, atmospheric muons, and cascades; this is described in Aartsen et al. (2019) and Aartsen et al. (2020).

For the analyses presented here, we focus on the full detector configuration of 86 strings spanning a time window from 2011 to 2018. Approximately 900,000 events from 2532 days are analyzed.

3. Likelihood Analyses

Many previous IceCube analyses searching for neutrino point sources relied on significant spatial clustering of IceCube data alone or significant association with known populations of astrophysical objects (Abbasi et al. 2011; Aartsen et al. 2013c, 2014b, 2016b, 2017a, 2019). Here we adopt the procedure described in Schumacher (2019) to search for counterparts to ANITA events. Namely, we perform three separate analyses to test different temporal hypotheses in the neutrino emission. Each of these analyses incorporates the information from the localization of the ANITA events through a joint likelihood. The sky is divided into grid positions, $\boldsymbol{x}_s$, and at each point, we maximize the likelihood, $\mathcal{L}$, with respect to the expected number of signal events, n_s, and other signal parameters contained in the variable α, depending on the different signal hypotheses tested, as described in Sections 3.2 and 3.3. This likelihood is given by

$$\mathcal{L} = \lambda \prod_{i=1}^{N} \left(\frac{n_s}{n_s + n_b} S(\boldsymbol{x}_i, \boldsymbol{x}_s, \boldsymbol{\alpha}) + \frac{n_b}{n_s + n_b} B(\boldsymbol{x}_i, \boldsymbol{x}_s \right) P_A(\boldsymbol{x}_s), \tag{1}$$

where n_b is the expected number of observed background events, and N is the total number of observed events in the time window. The vector $\boldsymbol{x}_i$ contains the event observables, such as reconstructed energy, direction, and reconstruction uncertainty, and P_A is the spatial probability distribution function (PDF) of ANITA events, which are included in Table 1. Here B describes the energy and decl. PDF of our background, which is the same among all analyses. Temporal terms in B are described in Sections 3.1 and 3.2. While the signal PDF S describes the signal hypothesis, the parameter λ modifies the likelihood formalism in order to take into account low-statistics problems in some of the analyses. In general, the signal PDF, S, is defined as

$$S = S^{\text{space}}(\boldsymbol{x}_i, \boldsymbol{x}_s, \boldsymbol{\sigma_i}) \cdot S^{\text{energy}}(E_i, \delta_i, \gamma) \cdot S^{\text{time}}. \tag{2}$$

These three terms reflect the spatial, energy, and time PDFs, respectively, of our signal hypothesis. The spatial term, S^{space}, expresses the probability for an event with a best-fit reconstructed direction $\boldsymbol{x}_i$ to originate from a source at the direction $\boldsymbol{x}_s$, according to a two-dimensional Gaussian function with angular resolution σ_i. The energy PDF S^{energy} describes the probability of obtaining an event with reconstructed energy E_i given a decl. δ_i under the hypothesis of an $E^{-\gamma}$ power-law energy spectrum, which helps differentiate signal from the known atmospheric backgrounds in our event selection. The time term, S^{time}, describes the time PDF of events observed from the source. While the spatial term is shared between all analyses, the energy and temporal terms are unique to each individual analysis. This joint likelihood procedure is carried out in three complementary search strategies: *prompt*, *rolling*, and *steady*.

3.1. Prompt

The first analysis searches for IceCube events in spatial coincidence with the ANITA events in short time windows, Δt, centered on each ANITA event. We call this period the *on-time window*. This is equivalent to setting S^{time} equal to a uniform PDF in this on-time window and zero for all times outside of this window. To help distinguish potential signals for time windows in which the expected number of background events is small, we set

$$\lambda = \frac{(n_s + n_b)^N}{N!} \cdot e^{-(n_s + n_b)}, \tag{3}$$

as in Aartsen et al. (2015a, 2018a). Due to the small statistics for short time windows, the likelihood is only maximized with respect to n_s, and the energy dependence in S^{energy} is fixed to an E^{-2} spectrum. To account for the temperature dependence of atmospheric muon rates (Aartsen et al. 2013d), we determine n_b by calculating the rate of events from the surrounding 5 days of data on either side of our on-time window. Taking the logarithmic likelihood ratio between the maximum likelihood and that of the null hypothesis results in our test statistic (TS), defined as

$$\text{TS} = -2\hat{n_s} + \sum_{i=1}^{N} 2\log\left[1 + \frac{\hat{n_s} S(\boldsymbol{x}_i, \boldsymbol{x}_s)}{n_b B(\boldsymbol{x}_i)}\right] + 2\log\left[\frac{P_A(\boldsymbol{x}_s)}{P_A(\boldsymbol{x}_0)}\right], \tag{4}$$

where $\mathbf{x}_0$ is the reported best-fit location of the ANITA event, and $\hat{n}_s$ is the value of n_s that maximizes the likelihood. The TS is calculated for all $\boldsymbol{x}_s$, and the maximum value is reported. For this analysis, P_A is a two-dimensional Gaussian assuming the localization uncertainties reported in Table 1. As we are not motivated by a specific astrophysical class of objects with characteristic timescales of emission, we consider constant emission over various time windows for each of the ANITA events. This technique is similar to previous IceCube searches for gamma-ray bursts and fast radio bursts (Aartsen et al. 2015a, 2018a). Because it

occurred before IceCube had attained a full detector configuration, AAE-061228 is excluded from this analysis. For AAC-150108, we consider three separate time windows: 10, 10^3, and 10^5 s. During the event time of AAE-141220, IceCube was temporarily not collecting data due to a run transition that had begun approximately 0.5 s before the event and lasting for about 1 minute. Because of this, we only investigate hypotheses of constant emission over two time windows (10^3 and 10^5 s), where the period of time from the run transition is not an appreciable portion of our on-time window.

3.2. Rolling

The second analysis also searches for temporal and spatial clustering of IceCube events but does not require the temporal coincidence between IceCube and ANITA events. In this untriggered analysis (Braun et al. 2010; Aartsen et al. 2015b), we assume a Gaussian time dependence to parameterize a limited duration increase in the emission of the source,

$$S^{\text{time}} = \frac{1}{\sqrt{2\pi}\sigma} e^{-\frac{(t_0 - t_i)^2}{2\sigma_t^2}}, \tag{5}$$

where t_0 and σ_t are the Gaussian mean time and Gaussian width of the flare, respectively. In the limit of large N, we are free to set λ to 1, and the increase in statistics allows us to fit for γ in the range $1 \leqslant \gamma \leqslant 4$ in addition to n_s, as is done in many previous IceCube analyses (Abbasi et al. 2011; Aartsen et al. 2013c, 2014b, 2016b, 2017a). Additionally, we set $n_s + n_b$ to be equal to the number of events, N. The TS for this analysis is then

$$\text{TS} = -2 \log \left[\frac{\text{T}}{\sqrt{2\pi}\hat{\sigma_t}} \times \frac{L(n_s = 0)}{\mathcal{L}(\hat{n_s}, \hat{\gamma}, \hat{\sigma_t}, \hat{t_0})} \right], \tag{6}$$

where $\hat{n_s}$, $\hat{\gamma}$, $\hat{\sigma_t}$, $\hat{t_0}$ are the best-fit values from the likelihood maximization and T is the total live time of the data-taking period. The multiplicative factor in front of the likelihood ratio in Equation (6) is a marginalization term to avoid undesired biases toward finding short flares, as explained in (Braun et al. 2010). The TS is calculated at the positions of a coarse sky grid ($1^\circ \times 1^\circ$ bin widths) built at the central coordinates of the ANITA events and covering 99.9% of the their two-dimensional spatial PDFs, but it sets P_A to be a uniform distribution covering this extended region. As the PDF is taken to be uniform in this analysis, there is no term in the TS that is dependent on P_A. The location of the maximum TS from the coarse search is then used as a seed to perform a further likelihood maximization, where the direction of the source, $\boldsymbol{x}_s$, is also reconstructed.

3.3. Steady

The third and final analysis tests for spatial clustering over 7 yr of IceCube data, assuming constant emission in the signal hypothesis, are done by setting S^{time} to be a uniform PDF over the entire data collection period. As in the rolling analysis, we take λ to be 1 and fit for γ in the likelihood maximization process. At all $\boldsymbol{x}_s$, we calculate the redefined TS,

$$\text{TS} = 2 \cdot \log \left[\frac{\mathcal{L}(\boldsymbol{x}_s, \hat{n}_s, \hat{\gamma})}{\mathcal{L}(\boldsymbol{x}_s, n_s = 0)} \right] + 2 \log \left[\frac{P_A(\boldsymbol{x}_s)}{P_A(\boldsymbol{x}_0)} \right], \tag{7}$$

with best-fit values $\hat{n}_s$ and $\hat{\gamma}$. The PDF of the ANITA events in this analysis is taken to be the same as in the prompt analysis, namely, a two-dimensional Gaussian.

4. Results

No significant correlation is found in any of the analyses above the expectation from background. In order to calculate p-values, the results are compared against pseudo-experiments from time-scrambled data (Aartsen et al. 2015b). The most significant observation results from the steady search for AAE-141220, with a p-value of 0.08 before trials correction.

Figure 1 displays the sky maps for the prompt, rolling, and steady analyses (left to right in the top panels) for AAE-141220. The bottom panels of Figure 1 show the comparison of the observed TS values for each analysis at the position of the red lines to their respective TS distributions from pseudo-experiments using time-scrambled data. Similar plots for AAE-061228 and AAC-150108 are displayed in Figure 6.

In the absence of a significant signal, upper limits (90% confidence level) for the time-integrated $\nu_\mu + \bar{\nu}_\mu$ flux are set for each ANITA event, where possible, using the prompt and steady analyses (Figure 2). To calculate upper limits, locations are sampled according to the per-event PDFs reported by ANITA, injecting the same level of flux at each sampled location, and running each iteration through the full analysis procedure, which maximizes the joint likelihood at all locations on the sky. This allows us to place upper limits on point sources whose locations are distributed according to the per-event PDF reported by ANITA. We set these limits for an assumed spectrum given by

$$\Phi(E, t) = \frac{dN_{\nu_\mu + \bar{\nu}_\mu}}{dE dA dt} = \Phi_0 \left(\frac{E}{E_0} \right)^{-2}, \tag{8}$$

where Φ_0 is a normalization constant on a point-source flux, which carries units of $\text{GeV}^{-1}\,\text{cm}^{-2}\,\text{s}^{-1}$. We constrain the time-integrated muon neutrino flux, E^2F, where

$$E^2F = E^2 \int \Phi(E, t) dt. \tag{9}$$

All of the limits we calculate are provided in Table 2. In the case where an upper limit fluctuates below the sensitivity, we conservatively set the upper limit to the sensitivity value. Prompt limits are placed at the specified time windows for emission centered on the ANITA event times, whereas limits from the steady analysis are for emission over the live time of our data sample. This hard spectrum was chosen conservatively because with the observation of EeV events by ANITA, if the underlying spectrum is softer, then the expected number of observable neutrinos for IceCube would increase. As the time-integrated flux sensitivity for the triggered analysis begins to worsen past 10^5 s, upper limits for $\Delta t > 10^5$ s are only set using the time-integrated approach.

5. Discussion

For many astrophysical sources, power-law spectra in photons are common over finite energy ranges. Additionally, diffusive shock acceleration models suggest that the neutrino spectrum, as well as gamma rays from pion decay, should follow a power-law spectrum, justifying the choice of testing

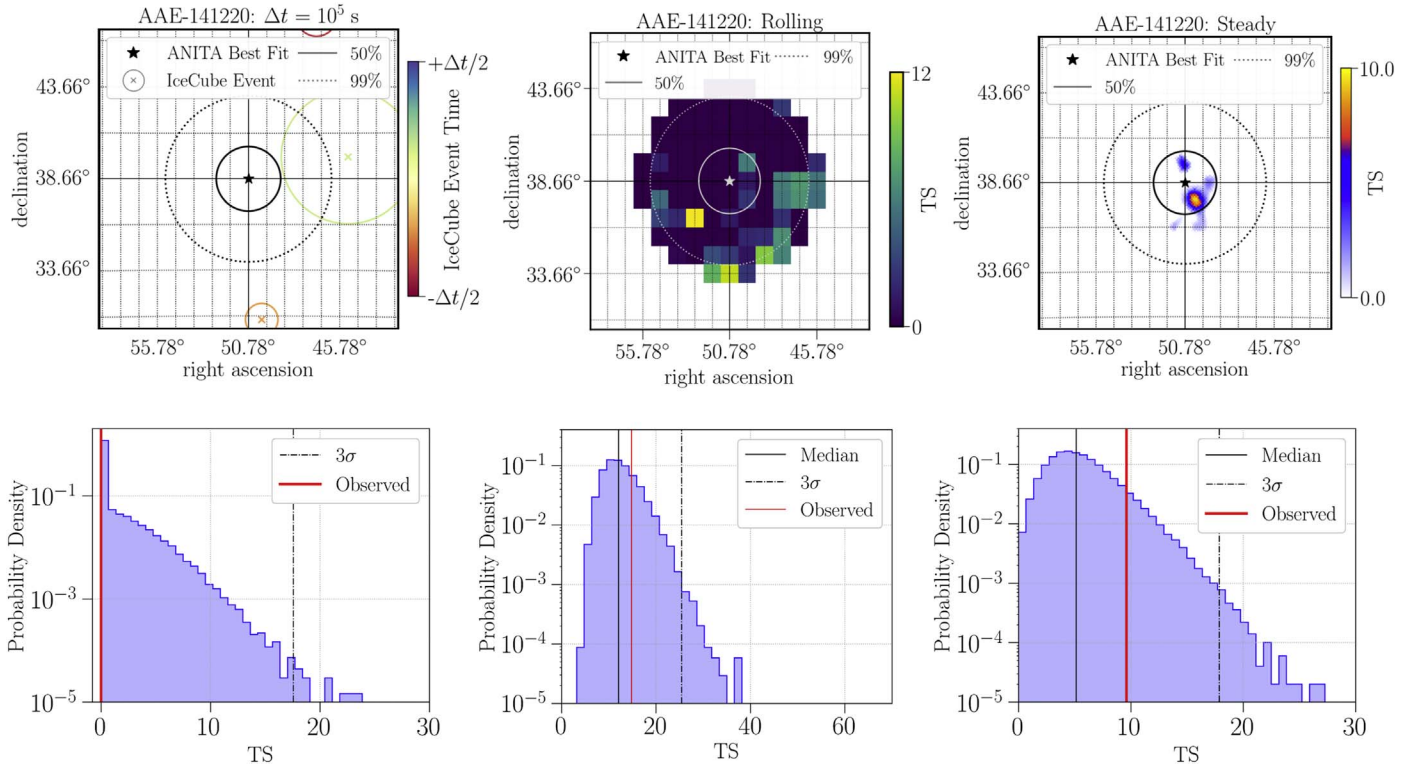

Figure 1. Sky maps (top) and TS distributions (bottom) for AAE-141220 for the prompt (left), rolling (middle), and steady (right) analyses. Observed TS values (shown in red) are compared to distributions from time-scrambled data realizations to quantify the significance. In all sky maps, solid (dotted) lines represent 50% (99%) containment of the reconstructed direction of the events. In the prompt analysis sky map, the best-fit location of each IceCube event is represented with a cross, and the size of the circle represents the uncertainty (50% containment) on the event's reconstruction, with color representing the IceCube event arrival time relative to the ANITA event. Both the sky map and TS distribution for this analysis are for the 10^5 s time window. In the rolling and steady analysis sky maps, color reflects the TS values defined in Sections 3.2 and 3.3 respectively.

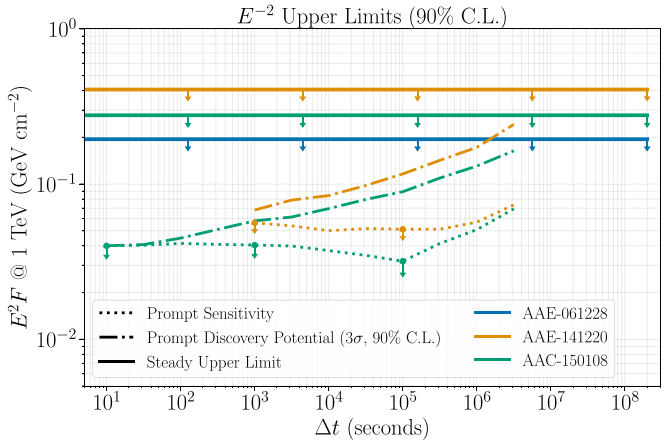

Figure 2. Sensitivity (dotted lines) and upper limits (arrows; 90% confidence level) on the time-integrated $\nu_\mu + \bar{\nu}_\mu$ flux normalization for an E^{-2} source spectrum as a function of Δt from the prompt analysis, compared to the upper limits (solid) from the steady analysis. The central 90% intervals of the expected neutrino energies for these spectra are 1 TeV–1 PeV. For the prompt analysis, we also include the discovery potential, which is the flux that results in a 3σ result, pretrials, in 90% of pseudo-experiments.

power laws for corresponding neutrino spectra. However, for the AAEs, interpolating a power law between the energy range at which IceCube is sensitive to the best-fit ANITA event energies could pose a problem. For soft spectra, events detected by ANITA would suggest that many events would be detectable at IceCube. For hard spectra, extrapolating between IceCube and ANITA would imply dramatic bolometric neutrino luminosities for any point source.

However, even in the case of non-power-law neutrino emission, the limits we can set on muon neutrinos in the TeV–PeV energy range can constrain the generic fluxes of incident tau neutrinos with EeV energies. As shown in Safa et al. (2020), any incident flux with an EeV ν_τ component that traverses large Earth chord lengths will result in a secondary flux of lower-energy neutrinos, to which IceCube would be sensitive. We use the same prescription here to analyze how constraining our limits are on a generic point-source flux that includes EeV neutrinos.

For any incident flux of neutrinos from the northern sky, $\Phi(E_\nu, t)$, the number of expected detected tau neutrino-induced muon events at IceCube is given by

$$\begin{aligned}\langle N^{\mu}_{\rm IceCube}\rangle = &\int dE_\mu \int dE_\tau \int dE_\nu \Phi(E_\nu, t) P^{\rm surv}_\tau(E_\nu) \\ &\times \frac{dN_\tau(E_\tau)}{dE_\tau}\frac{\Gamma_{\tau\to\mu}}{\Gamma_{\rm total}}\frac{dN_\mu}{dE_\mu}(E_\tau, E_\mu) A^{\mu}_{\rm eff}(E_\mu)\Delta T \\ &+ \int dE_\mu \int dE_\tau \int dE'_\nu \int dE_\nu \Phi(E_\nu, t) P_\nu(E_\nu, E'_\nu) \\ &\times \frac{dN_\nu}{dE'_\nu}(E'_\nu) N^p(E'_\nu)\frac{dN_\tau}{dE_\tau}(E'_\nu; E_\tau) \\ &\times \frac{\Gamma_{\tau\to\mu}}{\Gamma_{\rm total}}\frac{dN_\mu}{dE_\mu}(E_\tau; E_\mu) A^{\mu}_{\rm eff}(E_\mu)\Delta T, \end{aligned} \quad (10)$$

Table 2
Analysis Results and Upper Limits

Event	Analysis	Time Window	p-value	Upper Limit (GeV $\cdot$ cm^{-2})
AAE-061228	Steady	IC86-I–IC86-VII	0.606	0.195
	Rolling	IC86-I	0.562	⋯
		IC86-II–IC86-VII	0.208	⋯
AAE-141220		10 s	⋯	⋯
	Prompt	10^3 s	1.0	0.053
		10^5 s	1.0	0.051
	Steady	IC86-I–IC86-VII	0.081	0.401
	Rolling	IC86-I	0.342	⋯
		IC86-II–IC86-VII	0.224	⋯
AAC-150108		10 s	1.0	0.040
	Prompt	10^3 s	1.0	0.041
		10^5 s	1.0	0.032
	Steady	IC86-I–IC86-VII	0.210	0.278
	Rolling	IC86-I	0.636	⋯
		IC86-II–IC86-VII	0.512	⋯

Note. Upper limits (90% C.L.) are on the time-integrated $\nu_\mu + \bar{\nu}_\mu$ power-law flux (E^{-2}) from a point source following the spatial probability distribution provided by ANITA. Limits are set assuming constant emission over a fixed time window. As the temporal profile of emission is fit in the rolling analysis, no upper limits are placed from that analysis. Time windows for the steady and rolling analyses are listed as the IceCube seasons analyzed, where IC86-I contains 2.88×10^7 s of data and 1.90×10^8 s for IC86-II—IC86-VII. All p-values are not trial-corrected for the number of searches considered.

where the first contribution is from emerging τ-leptons that would decay to muons and then pass an IceCube event selection. The second contribution is from the remaining ν_τ flux, the majority of which has cascaded down in energy. The number of targets effectively seen by an incident neutrino with energy E_ν is N^p (E_ν). The effective area of this event selection to muons incident on the detector is displayed in Figure 3. Here $P_\tau^{\rm surv}(E_\nu)$ and P_ν (E_ν) represent the survival probability of a τ-lepton and ν_τ given an incident neutrino energy, respectively, and $\Gamma_{\tau\to\mu}/\Gamma_{\rm total}$ represents the branching ratio for the τ-decay to the muon channel, which is approximately 18%.

Similarly, for ANITA, the number of expected events from upgoing τ-leptons is given by

$$\langle N^\tau_{\rm ANITA}\rangle = \iint\left(dE_\nu dE'_\nu \Phi(E_\nu, t)\frac{dN(E'_\nu)}{dE'_\nu} \times \xi_{acc}(E'_\nu)\Delta T\right), \quad (11)$$

where $\xi_{\rm acc}$ represents ANITA's acceptance to τ-lepton air showers and is taken from Romero-Wolf et al. (2019). Values for the acceptance at angles that would require an incident neutrino to traverse a large column depth are set to the acceptance near the horizon. We take the value at an angle corresponding to the maximum acceptance before absorption effects dominate. This removes absorption effects in the reported acceptance, which is accounted for separately with the code used to propagate these fluxes, `TauRunner`, described in Safa et al. (2020, 2019). We focus our analysis

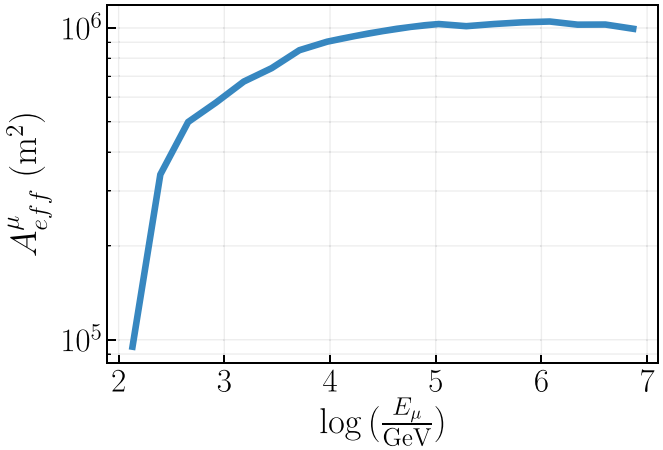

Figure 3. Effective area of the IceCube event selection to muons from the northern sky, incident on a volume 1.5 km away from the edge of the detector. The muon energy incident on this volume is E_μ.

on the nonobservation of coincident events in IceCube at $\Delta T = 10^3$ s. A similar procedure can be applied to longer time windows. Qualitatively, it would result in similar limits up to the lifetime of the ANITA flight. For longer emission timescales, limits from IceCube become even more constraining, as the implied normalization on the ANITA flux would have to increase to compensate for the fraction of time during which ANITA was not taking data.

To make as conservative a statement as possible, we inject fluxes described by delta-functions in energy, $\Phi(E_\nu, t) = \Phi_0\delta(E_\nu - E_0)$, where the normalization now carries units of cm^{-2}s^{-1}. After propagating these monoenergetic fluxes, we record what fraction of the incident flux results in a detectable signal at ANITA. We repeat this procedure for a variety of injected initial neutrino energies so that we can find the energy that yields the maximum probability of a τ-lepton arriving at ANITA with an energy within the quoted reconstructed energy bounds. We find that the optimal flux for ANITA corresponds to an injected ν_τ flux with $E_0 = 1$ EeV. Normalized cumulative distributions from secondary τ-leptons are shown in Figure 4 for injected neutrinos at angles corresponding to the best-fit reconstructed direction of AAE-141220.

We next inject a flux of EeV tau neutrinos and find the spectral shape of the secondary ν_τ flux that would be incident on IceCube. As we observed zero coincident events in the time window of 10^3 s around AAE-141220 in the prompt analysis, we calculate the maximum allowed flux normalization (at a 90% confidence level) on the primary flux that would evade this nonobservation. The results are displayed in Figure 5.

Although IceCube's sensitivity is peaked many orders of magnitude below the reconstructed energies of the AAEs, the limits set on any potential neutrino source that created AAE-141220 are more constraining by several orders of magnitude than the implied flux by the ANITA observations. If one considers constant emission over the entire live time of the IceCube event selection, then the time-integrated flux limit set by the IceCube nonobservation of AAE-141220 becomes around 1 order of magnitude less constraining, as is apparent in the steady limits in Figure 2. However, for the implied normalization placed by ANITA observations, this value would increase by approximately 2 orders of magnitude due to the limited live time of the ANITA flight. This has the overall

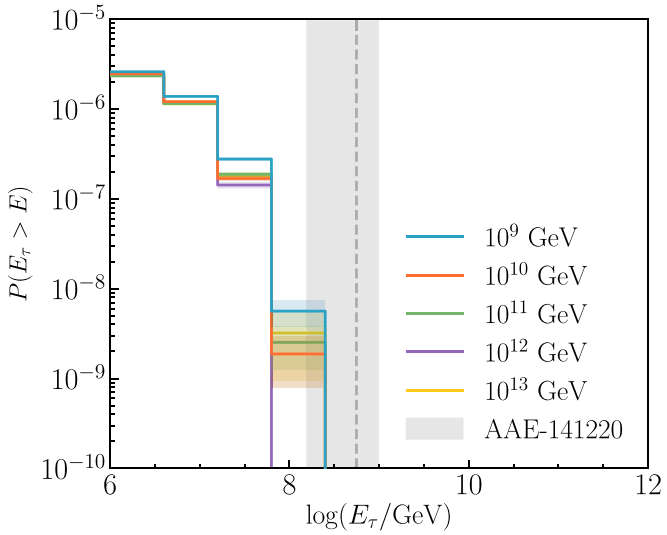

Figure 4. Normalized cumulative distributions for Earth-emerging τ-leptons. Colors correspond to the incoming τ-neutrino energy, and the gray band is the 95% containment on the error of the reconstructed shower energy of AAE-141220.

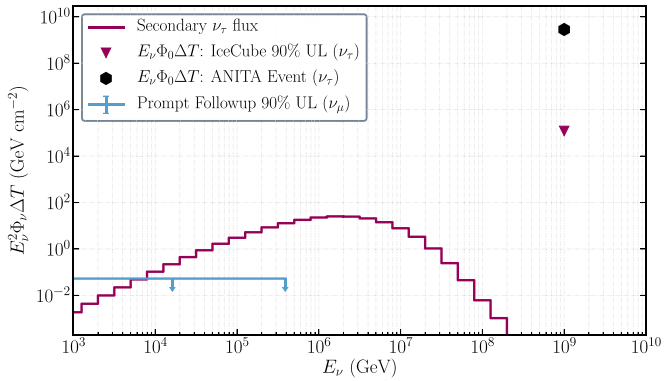

Figure 5. Upper limits (90% C.L.) placed by calculating the secondary neutrino flux (purple histogram) from an incident flux of EeV neutrinos assuming constant emission over 10^3 s and comparing to the nonobservation of IceCube events in the prompt analysis described in Section 3.1 for AAE-141220. The flux implied by the ANITA observations (black), represented in this figure as $E_\nu\Phi_0\Delta T = E_\nu\Delta T\int\Phi(E_\nu, t)dE_\nu$, using information about ANITA's acceptance (Romero-Wolf et al. 2019) overshoots this upper limit (purple arrow) by many orders of magnitude. For comparison, upper limits on the time-integrated muon neutrino flux from the prompt analysis are shown in blue. All fluxes are per flavor $\nu + \bar{\nu}$.

effect of increasing the tension between these two normalizations by approximately 1 more order of magnitude than for the 10^3 s follow-up shown in Figure 5. It is worth noting that the logic for scaling time-integrated limits also applies to AAE-061228, even though we cannot constrain the shorter timescales for this event. However, the emergence angle of this event at ANITA was shallower than that of AAE-141220, which increases the probability of observing such an event at ANITA by approximately 1 order of magnitude (Fox et al. 2018) for the same assumed initial flux; thus, the limit on assumed long-timescale emission would be about 1 order of magnitude less constraining than the case of AAE-141220.

If the intrinsic spectrum were to contain contributions from energies below 1 EeV, such as the power-law spectra tested in the analyses presented in Section 3, this would introduce a component to which IceCube might be sensitive but that could not produce events at ANITA consistent with the AAE; thus, this additional component would strengthen the constraints displayed in Figure 5. Additionally, if the spectrum consisted of neutrinos of energy greater than 1 EeV, the secondary ν_τ spectrum would have a similar shape to that shown in Figure 5, as discussed in Safa et al. (2020); therefore, the limits on the flux normalization would be constant for fluxes of higher energy, while the energy required to produce such a flux would scale with the injected energy. For that reason, these limits are conservative and severely constrain any incident spectrum that could produce an observable event at ANITA consistent with an AAE.

6. Conclusion

Recent detections of AAEs are considered anomalous due to the small survival probability of EeV tau neutrinos through long chord lengths. The events are known to be inconsistent with a cosmogenic interpretation but could have been produced by cosmic accelerators, specifically those with short characteristic timescales. We show here that for timescales as small as 10^3 s, assuming that AAE-141220 originated from a neutrino source, limits set using IceCube data are more than 4 orders of magnitude in tension with the point-source flux required to detect one event at ANITA. These limits are constraining for a variety of flux models, from simple power laws to any generic model that includes a component at or above EeV energies. In addition to the anomalous events, we also find no evidence for a neutrino source in the direction of the neutrino candidate event from a search for Askaryan emission during ANITA-III. As searches for Askaryan emission with ANITA have targeted a diffuse UHE cosmic neutrino flux (Gorham et al. 2018a) and not localized point-source fluxes, studies that quantify the acceptance of the ANITA detector (Cremonesi et al. 2019) focus on diffuse acceptances and not effective areas for neutrino fluxes from fixed locations on the sky. For this reason, we do not provide a comparison between the limits we set here and potential implications for point-source fluxes based on the observation of the AAC. With knowledge of the effective area of ANITA in the direction of the AAC, and assuming that any astrophysical flux were of roughly equal flavor upon reaching Earth, the same secondary ν_τ analysis could be performed for the AAC. However, constraints from such a search would be considerably weaker than those for the AAE, as the AAC was Earth-skimming, and thus a greater fraction of any high-energy incident flux would be able to reach the ANITA detector prior to interacting deep within the Earth. Therefore, this method of using secondary ν_τ fluxes from UHE neutrinos in IceCube could be beneficial for future correlation searches with radio detectors and future Cerenkov detectors such as POEMMA (Venters et al. 2019).

These new limits, in conjunction with the inconsistency of isotropic flux interpretations, leave no room for an astrophysical interpretation of AAEs in the context of the standard model for time windows as short as 10^3 s. However, it has been shown that these events can be explained using physics beyond the standard model, as many models suggest that AAEs lend support for axionic dark matter, sterile neutrinos, supersymmetry, or heavy dark matter (Anchordoqui et al. 2018; Connolly et al. 2018; Dudas et al. 2018; Fox et al. 2018; Huang 2018; Abdullah et al. 2019; Anchordoqui & Antoniadis 2019; Borah et al. 2019; Chauhan & Mohanty 2019; Cherry & Shoemaker 2019; Chipman et al. 2019; Cline et al. 2019;

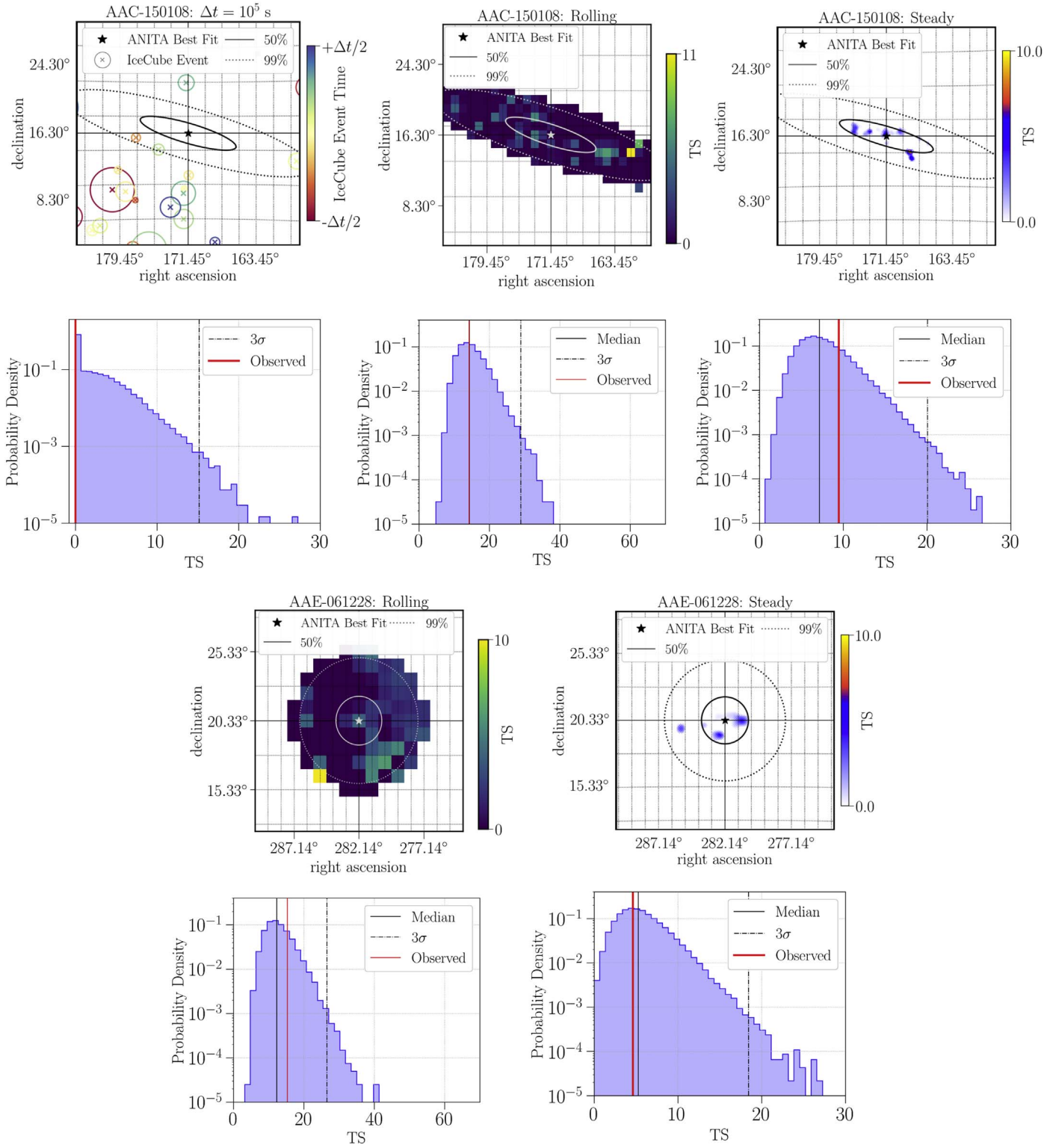

Figure 6. (Top two rows) Sky maps and TS distributions from all three analyses for AAC-150108. For AAE-061228, IceCube was not in a full detector configuration at the time of the event, and thus only the steady and rolling analyses were used to search for neutrino emission. Sky maps and TS distributions for these analyses are displayed in the bottom two rows.

Collins et al. 2019; Esmaili & Farzan 2019; Esteban et al. 2019; Heurtier et al. 2019a, 2019b; Hooper et al. 2019). Many of these models, excluding the axionic dark matter explanation (Esteban et al. 2019) or those heavy dark matter scenarios that are tuned to prevent signatures in IceCube (Hooper et al. 2019), can be constrained by this nonobservation at IceCube. Dedicated tests to quantify these constraints are beyond the scope of this work and may be the focus of a future study. In addition to explanations that incite new physics, it has recently been suggested that AAEs could be explained by downward-going CR-induced EASs that reflected off of subsurface features in the Antarctic ice (Shoemaker et al. 2019). Another

possible explanation could be coherent transition radiation from the geomagnetically induced air shower current, which could mimic an upgoing air shower (Motloch et al. 2017; de Vries & Prohira 2019). Explaining these anomalous events with systematic effects or confirming the need for new physics requires a deeper understanding of ANITA's detection volume. Efforts such as the HiCal radio frequency pulser, which has flown alongside ANITA on the last two flights (Prohira et al. 2018), are already underway to try to characterize the various properties of the Antarctic ice surface.

The IceCube collaboration acknowledges the significant contributions to this manuscript from Anastasia Barbano, Alex Pizzuto, and Ibrahim Safa. The authors gratefully acknowledge support from the following agencies and institutions: USA: U.S. National Science Foundation–Office of Polar Programs, U.S. National Science Foundation–Physics Division, Wisconsin Alumni Research Foundation, Center for High Throughput Computing (CHTC) at the University of Wisconsin–Madison, Open Science Grid (OSG), Extreme Science and Engineering Discovery Environment (XSEDE), U.S. Department of Energy–National Energy Research Scientific Computing Center, particle astrophysics research computing center at the University of Maryland, Institute for Cyber-Enabled Research at Michigan State University, and astroparticle physics computational facility at Marquette University; Belgium: Funds for Scientific Research (FRS-FNRS and FWO), FWO Odysseus and Big Science programs, and Belgian Federal Science Policy Office (Belspo); Germany: Bundesministerium für Bildung und Forschung (BMBF), Deutsche Forschungsgemeinschaft (DFG), Helmholtz Alliance for Astroparticle Physics (HAP), Initiative and Networking Fund of the Helmholtz Association, Deutsches Elektronen Synchrotron (DESY), and High Performance Computing Cluster of the RWTH Aachen; Sweden: Swedish Research Council, Swedish Polar Research Secretariat, Swedish National Infrastructure for Computing (SNIC), and Knut and Alice Wallenberg Foundation; Australia: Australian Research Council; Canada: Natural Sciences and Engineering Research Council of Canada, Calcul Québec, Compute Ontario, Canada Foundation for Innovation, WestGrid, and Compute Canada; Denmark: Villum Fonden, Danish National Research Foundation (DNRF), Carlsberg Foundation; New Zealand: Marsden Fund; Japan: Japan Society for Promotion of Science (JSPS) and Institute for Global Prominent Research (IGPR) of Chiba University; Korea: National Research Foundation of Korea (NRF); Switzerland: Swiss National Science Foundation (SNSF); United Kingdom: Department of Physics, University of Oxford.

ORCID iDs

M. Ahlers https://orcid.org/0000-0003-0709-5631
E. Bernardini https://orcid.org/0000-0003-3108-1141
P. Dave https://orcid.org/0000-0002-3879-5115
J. J. DeLaunay https://orcid.org/0000-0001-5229-1995
P. Desiati https://orcid.org/0000-0001-9768-1858
P. A. Evenson https://orcid.org/0000-0001-7929-810X
D. Fox https://orcid.org/0000-0002-3714-672X
A. Franckowiak https://orcid.org/0000-0002-5605-2219
J. Gallagher https://orcid.org/0000-0001-8608-0408
S. Garrappa https://orcid.org/0000-0003-2403-4582
T. Glüsenkamp https://orcid.org/0000-0002-2268-9297
D. Kang https://orcid.org/0000-0002-5149-9767
U. Katz https://orcid.org/0000-0002-7063-4418
A. Kheirandish https://orcid.org/0000-0001-7074-0539
N. Park https://orcid.org/0000-0002-4282-736X
A. Pizzuto https://orcid.org/0000-0002-8466-8168
M. Santander https://orcid.org/0000-0001-7297-8217
N. L. Strotjohann https://orcid.org/0000-0002-4667-6730
J. Vandenbroucke https://orcid.org/0000-0002-9867-6548

References

Aab, A., Abreu, P., Aglietta, M., et al. 2015, PhRvD, 91, 092008
Aartsen, M. G., Abbasi, R., Abdou, Y., et al. 2013a, Sci, 342, 1242856
Aartsen, M. G., Abbasi, R., Abdou, Y., et al. 2013b, NIMPA, 711, 73
Aartsen, M. G., Abbasi, R., Abdou, Y., et al. 2013c, ApJ, 779, 132
Aartsen, M. G., Abbasi, R., Abdou, Y., et al. 2013d, arXiv:1309.7003
Aartsen, M. G., Abbasi, R., Abdou, Y., et al. 2014a, NIMPA, 736, 143
Aartsen, M. G., Ackermann, M., Adams, J., et al. 2014b, ApJ, 796, 109
Aartsen, M. G., Ackermann, M., Adams, J., et al. 2015a, ApJ, 805, L5
Aartsen, M. G., Ackermann, M., Adams, J., et al. 2015b, ApJ, 807, 46
Aartsen, M. G., Abraham, K., Ackermann, M., et al. 2016a, PhRvL, 117, 241101 [Erratum: 2017, PhRvL, 119, 259902]
Aartsen, M. G., Abraham, K., Ackermann, M., et al. 2016b, ApJ, 824, L28
Aartsen, M. G., Abraham, K., Ackermann, M., et al. 2017a, ApJ, 835, 151
Aartsen, M. G., Ackermann, M., Adams, J., et al. 2017b, JINST, 12, P03012
Aartsen, M. G., Ackermann, M., Adams, J., et al. 2018a, ApJ, 857, 117
Aartsen, M. G., Ackermann, M., Adams, J., et al. 2018b, PhRvD, 98, 062003
Aartsen, M. G., Ackermann, M., Adams, J., et al. 2018c, Sci, 361, eaat1378
Aartsen, M. G., Ackermann, M., Adams, J., et al. 2018d, Sci, 361, 147
Aartsen, M. G., Ackermann, M., Adams, J., et al. 2019, EPJC, 79, 234
Aartsen, M. G., Ackermann, M., Adams, J., et al. 2020, PhRvL, 124, 051103
Abbasi, R., Abdou, Y., Abu-Zayyad, T., et al. 2010, NIMPA, 618, 139
Abbasi, R., Abdou, Y., Abu-Zayyad, T., et al. 2011, ApJ, 732, 18
Abbasi, R., Ackermann, M., Adams, J., et al. 2009, NIMPA, 601, 294
Abdullah, M., Dutta, B., Ghosh, S., & Li, T. 2019, PhRvD, 100, 115006
Achterberg, A., Ackermann, M., Adams, J., et al. 2006, APh, 26, 155
Ahrens, J., Bai, X., Bay, R., et al. 2004, NIMPA, 524, 169
Anchordoqui, L. A., & Antoniadis, I. 2019, Phys. Lett., B790, 578
Anchordoqui, L. A., Barger, V., Learned, J. G., Marfatia, D., & Weiler, T. J. 2018, LHEP, 1, 13
Askar'yan, G. A. 1962, JETP, 14, 441
Borah, D., Dasgupta, A., Dey, K., & Tomar, G. 2019, arXiv:1907.02740
Braun, J., Baker, M., Dumm, J., et al. 2010, APh, 33, 175
Carver, T. 2019, arXiv:1908.05993
Chauhan, B., & Mohanty, S. 2019, PhRvD, 99, 095018
Cherry, J. F., & Shoemaker, I. M. 2019, PhRvD, 99, 063016
Chipman, S., Diesing, R., Reno, M. H., & Sarcevic, I. 2019, PhRvD, 100, 063011
Cline, J. M., Gross, C., & Xue, W. 2019, PhRvD, 100, 015031
Collins, J. H., Bhupal Dev, P. S., & Sui, Y. 2019, PhRvD, 99, 043009
Connolly, A., Allison, P., & Banerjee, O. 2018, arXiv:1807.08892
Cremonesi, L., Connolly, A., Allison, P., et al. 2019, JINST, 14, P08011
de Vries, K. D., & Prohira, S. 2019, PhRvL, 123, 091102
Dudas, E., Gherghetta, T., Kaneta, K., Mambrini, Y., & Olive, K. A. 2018, PhRvD, 98, 015030
Esmaili, A., & Farzan, Y. 2019, JCAP, 1912, 017
Esteban, I., Lopez-Pavon, J., Martinez-Soler, I., & Salvado, J. 2019, arXiv:1905.10372
Fox, D. B., Sigurdsson, S., Shandera, S., et al. 2018, PhRvD, submitted (arXiv:1809.09615)
Gaisser, T. K., Halzen, F., & Stanev, T. 1995, PhR, 258, 173 [Erratum: 1996, PhR, 271, 355]
Gorham, P. W., Allison, P., Barwick, S. W., et al. 2009, APh, 32, 10
Gorham, P. W., Nam, J., Romero-Wolf, A., et al. 2016, PhRvL, 117, 071101
Gorham, P. W., Allison, P., Banerjee, O., et al. 2018a, PhRvD, 98, 022001
Gorham, P. W., Rotter, B., Allison, P., et al. 2018b, PhRvL, 121, 161102
Greisen, K. 1966, PhRvL, 16, 748
Haack, C., & Wiebusch, C. 2018, ICRC (Busan), 301, 1005
Heurtier, L., Kim, D., Park, J.-C., & Shin, S. 2019a, PhRvD, 100, 055004
Heurtier, L., Mambrini, Y., & Pierre, M. 2019b, PhRvD, 99, 095014
Hooper, D., Wegsman, S., Deaconu, C., & Vieregg, A. 2019, PhRvD, 100, 043019
Hoover, S., Nam, J., Gorham, P. W., et al. 2010, PhRvL, 105, 151101

Huang, G.-y. 2018, PhRvD, 98, 043019
Motloch, P., Alvarez-Muñiz, J., Privitera, P., & Zas, E. 2017, PhRvD, 95, 043004
Prohira, S., Novikov, A., Dasgupta, P., et al. 2018, PhRvD, 98, 042004
Romero-Wolf, A., Wissel, S. A., Schoorlemmer, H., et al. 2019, PhRvD, 99, 063011
Safa, I., Pizzuto, A., Argüelles, C. A., et al. 2020, JCAP, 2001, 012
Safa, I., Pizzuto, A., Argüelles, C. A., et al. 2019, ICRC (Madison, WI), 36, 995
Schumacher, L. 2019, EPJWC, 207, 02010
Shoemaker, I. M., Kusenko, A., Munneke, P. K., et al. 2019, arXiv:1905.02846
Venters, T. M., Reno, M. H., Krizmanic, J. F., et al. 2019, arXiv:1906.07209
Zas, E. 2018, ICRC (Busan), 301, 972
Zatsepin, G. T., & Kuzmin, V. A. 1966, JETPL, 4, 78